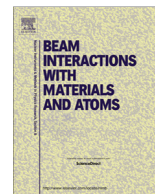




Contents lists available at ScienceDirect

Nuclear Instruments and Methods in Physics Research B

journal homepage: www.elsevier.com/locate/nimb

Electron–lattice coupling after high-energy deposition in aluminum

S.A. Gorbunov^a, N.A. Medvedev^b, P.N. Terekhin^c, A.E. Volkov^{c,a,d,*}^a Lebedev Physical Institute of the Russian Academy of Sciences, Leninskij pr. 53, 119991 Moscow, Russia^b Center for Free-Electron Laser Science at DESY, Notkestr. 85, 22607 Hamburg, Germany^c National Research Centre 'Kurchatov Institute', Kurchatov Sq. 1, 123182 Moscow, Russia^d Joint Institute for Nuclear Research, Joliot-Curie 6, 141980 Dubna, Moscow Region, Russia

ARTICLE INFO

Article history:

Received 14 July 2014

Accepted 17 November 2014

Available online xxx

Keywords:

Electron–lattice coupling

Dynamic-structure factor

Ion track

Laser spot

ABSTRACT

This paper presents an analysis of the parameters of highly-excited electron subsystem of aluminum, appearing e.g. after swift heavy ion impact or laser pulse irradiation. For elevated electron temperatures, the electron heat capacity and the screening parameter are evaluated. The electron–phonon approximation of electron–lattice coupling is compared with its precise formulation based on the dynamic structure factor (DSF) formalism. The DSF formalism takes into account collective response of a lattice to excitation including all possible limit cases of this response. In particular, it automatically provides realization of electron–phonon coupling as the low-temperature limit, while switching to the plasma-limit for high electron temperatures. Aluminum is chosen as a good model system for illustration of the presented methodology.

© 2014 Elsevier B.V. All rights reserved.

1. Introduction

High energy deposition into a solid by swift heavy ions decelerated in the electronic stopping regime (SHI, $M > 20 m_p$, $E > 1$ MeV/amu, m_p is a proton mass) allows to achieve extreme levels of excitation of its electron subsystem. The temperature of the electron ensemble can rise up to several Fermi energies in the nanometric vicinity of the ion trajectory (SHI track) at the femto- to pico-second timescale after an ion passage [1,2]. Similar levels of electronic excitations are reached on the micrometer scale during irradiations of solids with femtosecond free-electron lasers (FEL) [3–6]. Subsequent relaxations of the excited electron subsystem results in energy and momentum transfer into the lattice that may lead to unusual nanometric structural and phase transformations in an irradiated material [1–6].

Taking into account fast and large increase of the temperature of delocalized electrons appearing after high energy deposition, the Two Temperature (Thermal Spike) Model (TTM, TSM) is often used to describe possible lattice heating by the ensemble of hot electrons [1,2]. The relative “simplicity” of TTM provides its popularity in the society [1,2].

However, macroscopic models or fitting procedures are often applied to determine the key parameters of TTM, e.g. the

dependence of the electron–lattice coupling factor on the temperature of the ensemble of delocalized electrons. Taking into account the ultrashort temporal and spatial scales of TTM in SHI tracks, such choosing of the parameters may stimulate reasonable doubts in results of application of the model to simulations of lattice excitation (see, e.g. [7,8] or [9,10]).

This paper is aimed to supply researchers using TTM with these parameters calculated rigorously. Aluminum was chosen as a model system for demonstration of these dependencies. The main efforts are focused on the dependence of the electron–lattice coupling factor on the temperature of the ensemble of delocalized electrons generated in a SHI track. The electron–phonon mechanism is often used to describe electron lattice coupling in SHI tracks/laser spots. However, the time of cooling of the electronic subsystem of a solid in a nanometric SHI track is shorter than, or on the order of, the characteristic time of atomic oscillations in a lattice [7–10]. This makes an application of the electron–phonon mechanism questionable for the description of interaction of hot electrons with a lattice in a SHI track. We compare results of applications of the electron–phonon approximation with the general formulation of electron–lattice coupling based on the dynamic structure factor (DSF) formalism [11]. DSF takes into account in a quantitative way effects of all the spectrum of spatial and temporal correlations in the atomic dynamics on lattice excitation. In particular, it automatically provides realization of electron–phonon mechanism as the low-temperature limit, while switching to the plasma-limit for high electron temperatures.

* Corresponding author at: National Research Centre 'Kurchatov Institute', Kurchatov Sq. 1, 123182 Moscow, Russia.

E-mail address: a.e.volkov@list.ru (A.E. Volkov).

The molecular dynamics (MD) procedure is developed to calculate the DSF and to simulate the kinetics of lattice excitations at the sub-picosecond timescales as well as to obtain the dependence of the electron–lattice energy transfer rate on the electron temperature. Additionally, the other necessary parameters for the TTM, namely the electron heat capacity and the screening parameter as functions of electron temperature are obtained taking into account the realistic density of states of solid aluminum.

2. Electron–lattice energy transfer rate, electron heat capacity and screening in aluminum

Due to the screening effect and high Fermi energy, the kinetic energies of conduction-band electrons in aluminum are larger than the energies of their interaction, and the one-electron approximation can be used to describe the state of this electron ensemble. The rate of electron–lattice energy exchange, Q_{e-i} , is given by the moment of the one-electron kinetic equation [9]:

$$Q_{e-i} = \frac{\hbar^3}{2\pi^3 m_e^2} \int f_{\mathbf{k}_i} (1 - f_{\mathbf{k}_f}) \hbar \omega \frac{k_i}{k_f} \frac{\partial^2 \sigma}{\partial \Omega \partial (\hbar \omega)} d\mathbf{k}_i d\mathbf{k}_f. \quad (1)$$

Here σ is the cross section of an electron scattering on the ion subsystem; $f_{\mathbf{k}}$ is the distribution functions of electrons ($f_{\mathbf{k}} = f_{\mathbf{k}}^{eq}$ is the Fermi function in case of local equilibrium); Ω is the solid angle of electron scattering; \mathbf{k}_i and \mathbf{k}_f are the initial and final wave vectors of an electron; $\hbar \omega = \frac{\hbar^2 \mathbf{k}_f^2}{2m_e} - \frac{\hbar^2 \mathbf{k}_i^2}{2m_e}$ is the change of the energy in the free-electron approximation, which works very well for aluminum; m_e is the free-electron mass.

The first Born approximation is applicable when describing coupling of a lattice with the excited ensemble of delocalized electrons in a SHI track [10]. Within this approximation, the differential cross section is factored into the cross section of electron scattering on an isolated atom and the “charge–charge” dynamic structure factor (DSF) of a target. DSF describes effects of spatial and temporal correlations in positions and dynamics of lattice atoms on electron scattering [11]:

$$\frac{\partial^2 \sigma}{\partial \Omega \partial (\hbar \omega)} = |V(\mathbf{k})|^2 \frac{m_e^2}{4\pi^2 \hbar^5} \frac{k_f}{k_i} S(\mathbf{k}, \omega). \quad (2)$$

Here $V(\mathbf{k})$ is the spatial Fourier transform of the interaction potential between an electron and a single atom of a target; $\mathbf{k} = \mathbf{k}_i - \mathbf{k}_f$ is the change of the wave vector of a scattered electron.

The Fourier transform of the atomic spatial and temporal pair correlation function $G(\mathbf{r}, t)$ determines the DSF [11]:

$$S(\mathbf{k}, \omega) = \frac{N}{2\pi} \int dt d\mathbf{r} \exp[i(\mathbf{k}\mathbf{r} - \omega t)] G(\mathbf{r}, t). \quad (3)$$

where N is the number of scattering atoms.

In the classical approximation of the lattice dynamics, $G(\mathbf{r}, t)$ is reduced to the simple form [12]:

$$G(\mathbf{r}, t) = \frac{1}{N} \left\langle \sum_{ij=1}^N \delta(\mathbf{r} + \mathbf{R}_i(0) - \mathbf{R}_j(t)) \right\rangle. \quad (4)$$

where $\mathbf{R}_i(0)$ is a coordinate of an i -th atom at the initial time, $\mathbf{R}_j(t)$ is a coordinate of a j -th atom at the time instance t , $\langle \dots \rangle$ is a statistical averaging over the atomic ensemble. The following correction should be introduced into the classical DSF $S_{cl}(\mathbf{k}, \omega)$ in order to satisfy the necessary quantum–mechanical asymmetry [13–16]:

$$S(\mathbf{k}, \omega) = \frac{(\hbar \omega / T_l)}{1 - \exp[-(\hbar \omega / T_l)]} S_{cl}(\mathbf{k}, \omega). \quad (5)$$

where T_l is the lattice temperature

Combining Eqs. (1)–(5), the following formula for the energy transfer rate can be obtained:

$$Q_{e-i} = - \frac{4}{(2\pi)^5 \hbar^2} \int d\mathbf{k}_i d\mathbf{k}_f E_{\mathbf{k}_i} |V(\mathbf{k})|^2 \left[f_{\mathbf{k}_f}^{eq} (1 - f_{\mathbf{k}_i}^{eq}) S(-\mathbf{k}, -\omega) - f_{\mathbf{k}_i}^{eq} (1 - f_{\mathbf{k}_f}^{eq}) S(\mathbf{k}, \omega) \right], \quad (6)$$

where $E_{\mathbf{k}} = (\hbar^2 \mathbf{k}^2) / 2m_e$ is the energy of an electron. The Fermi function $f_{\mathbf{k}}^{eq}(T_e)$ is used to describe the electron ensemble at different temperatures.

Eq. (6) demonstrates that the calculation of the energy transfer rate needs the electron temperature dependencies of the interaction potential (screening length $L_s(T_e)$) and the chemical potential of the electron ensemble. Realization of TTM model also requires knowledge about such dependencies of the electron heat capacity, $C_e(T_e)$, and the electron heat conductivity. The last one is beyond the scope of the present paper.

The density of states (DOS, $D(E)$) of the ensemble of delocalized electrons in a material determines the forms of these dependencies. We took the realistic DOS of aluminum from [17], where it is normalized to 3 electrons per aluminum atom.

Below we present the dependencies of the electron heat capacity and the screening lengths on the temperature of the electron ensemble in the conduction band of aluminum. The temperature dependence of the chemical potential $\mu(T_e)$ we calculated coincides exactly with that given in [17].

The electron heat capacity is determined by:

$$C_e(T_e) = \int_0^\infty \frac{\partial f(E, T_e, \mu(T_e))}{\partial T_e} D(E) E dE. \quad (7)$$

Numerical solution of Eq. (7) gives the temperature dependence of $C_e(T_e)$ presented in Fig. 1. This dependence is close to that obtained from DOS of a free electrons gas. Deviations between these dependencies occur at low temperatures, where effects from peculiarities of DOS structure are more pronounced. The electron heat capacity in [17] underestimates the temperature dependency of $C_e(T_e)$.

The screened Coulomb potential (Yukawa potential [18]) was chosen to describe the interaction of an electron with a lattice atom:

$$V(r) = Z \frac{e^2}{r} e^{-r/L_s}. \quad (8)$$

Here e is the electron charge, $Z \cdot e$ is the charge of a lattice ion, L_s is the screening length determined according to [19–21] as:

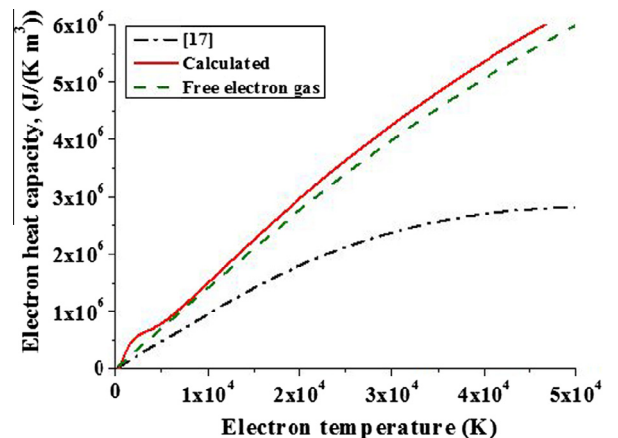


Fig. 1. Calculated electron heat capacity in aluminum vs those calculated in [17] and free electron gas approximation.

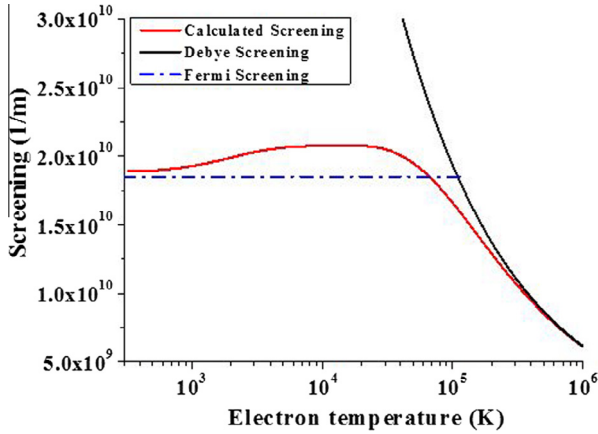


Fig. 2. Temperature dependence of the calculated screening parameter in the ensemble of conduction band electrons in aluminum vs Debye screening (black dashed curve) and Fermi screening (blue dash-dotted curve). (For interpretation of the references to color in this figure legend, the reader is referred to the web version of this article.)

$$k_{sc}^2 = L_S^{-2} = \frac{e^2}{\epsilon_0} \int_0^\infty \left| \frac{\partial f(E)}{\partial E} \right| D(E) dE. \quad (9)$$

Here k_{sc} is the inverse screening length, and ϵ_0 is the vacuum permittivity in the SI units. Eq. (9) automatically produces the limit cases of the screening at low and high electron temperatures:

$$k_{sc}^2 = \begin{cases} (e^2/\epsilon_0) \times D(E_f), & \text{Fermi-screening } (T_e \ll E_f) \\ e^2 n_e / \epsilon_0 T_e, & \text{Debye-screening } (T_e \gg E_f) \end{cases}. \quad (10)$$

In case of the free-electron gas, the low-temperature limit can be rewritten in a more familiar form of the Fermi-screening as $k_{sc}^2 = (e^2 m_e k_f) / (\epsilon_0 \pi^2 \hbar^2)$, taking into account the value of DOS at $E = E_f$. The temperature dependence of the screening as well as its high- and low-temperature limits for conduction band electrons of aluminum are presented in Fig. 2.

It should be noted that the results from [19] are higher than ours by a factor of $\sqrt{2}$. It should be also mentioned that as described in [22], coupled electron–lattice modes can contribute as an additional screening. Thus, we will analyse below an effect of such increased screening on electron–lattice coupling.

3. Limit cases of dynamical response of a lattice to excitation

Two main limit cases of dynamical reaction of coupled ensemble of atoms to excitation can occur depending on the interaction time of an incident electron with a dynamically coupled lattice volume [11].

3.1. Instantaneous approximation

When the interaction time of an electron with a dynamically coupled lattice volume is shorter than the characteristic time of correlation in the atomic dynamics (atomic oscillation (phonon) time), the DSF can be written in the instantaneous approximation assuming the lattice as dynamically independent atoms frozen in their current positions [11]:

$$S_{inst}(\mathbf{k}, \omega) = S(\mathbf{k})\delta(\omega) - S_{id}(\mathbf{k})\delta(\omega) + S_{id}(\mathbf{k}, \omega). \quad (11)$$

Here $S(\mathbf{k}) = \int S(\mathbf{k}, \omega) d\omega$ is a geometrical structure factor of a lattice, and S_{id} the ideal-gas DSF which can be obtained by the asymmetrization (see Eq.(5)) of its classical approximation [23]:

$$S_{id}^cl(\mathbf{k}, \omega) = \sqrt{\frac{M}{2\pi T_i k^2}} \exp\left(-\frac{M\omega^2}{2T_i k^2}\right). \quad (12)$$

3.2. Harmonic (phonons) approximation

When the time of interaction with a dynamically coupled lattice volume is longer than the atomic oscillation (phonon) time, DSF can be calculated assuming small harmonic oscillations of lattice atoms near their equilibrium positions [24]:

$$S^{ph}(\mathbf{k}, \omega) = \frac{A\hbar k^2 e^{-2W_{DW}}}{2N_{cell}M} \sum_{\xi_i=1}^p \sum_{\xi_j=1}^p e^{-i\mathbf{k}(\mathbf{r}_{\xi_i}-\mathbf{r}_{\xi_j})} \times \sum_{\mathbf{q}} \frac{1}{\omega_{\mathbf{q}}} \left[\delta(\omega + \omega_{\mathbf{q}}) n_{\mathbf{q}} \sum_{n_i=1}^{N_{cell}} \sum_{n_j=1}^{N_{cell}} e^{-i(\mathbf{k}+\mathbf{q})(\mathbf{R}_{n_i}-\mathbf{R}_{n_j})}, \right. \\ \left. + \delta(\omega - \omega_{\mathbf{q}}) (n_{\mathbf{q}} + 1) \sum_{n_i=1}^{N_{cell}} \sum_{n_j=1}^{N_{cell}} e^{-i(\mathbf{k}-\mathbf{q})(\mathbf{R}_{n_i}-\mathbf{R}_{n_j})} \right] \quad (13)$$

where \mathbf{R}_{n_i} is the position of n_i -th unit cell; \mathbf{r}_{ξ_i} is the equilibrium position of ξ_i -th atom in the n_i -th unit cell; the indices n_i and n_j are varying from 1 to the number of unit cells N_{cell} ; the indices ξ_i and ξ_j are running from 1 to p , the number of atoms in the unit cell; $n_{\mathbf{q}}$ is the number of occupied phonon states characterized by the wave vector \mathbf{q} ; M is a mass of a lattice atom. The quantity A is defined as

$$A = \frac{1}{k^2} \sum_{\lambda} |\mathbf{k}e^{(\lambda)}|^2, \quad (14)$$

which gives $A = 4$ for aluminum within the assumed independence of the phonon polarization vector $e^{(\lambda)}$ from the index μ . W_{DW} is the Debye–Waller factor:

$$W_{DW} = \frac{A\hbar k^2}{2MN_{cell}} \sum_{\mathbf{q}} \frac{1}{\omega(\mathbf{q})} \left[n(\mathbf{q}) + \frac{1}{2} \right]. \quad (15)$$

As it will be demonstrated below, the MD model and numerical technique applied in this paper take automatically into account realizations of these two limit cases, as well as other cases of the dynamical response of the lattice interacting with a relaxing ensemble of electrons characterized by different temperatures.

4. Electron–phonon energy transfer rate

In order to compare our results with those of other groups we repeated calculations made in [19] for a wide range of electron temperatures. The rate of the energy transfer determined there in the framework of the electron–phonon coupling model (see details in [19]):

$$Q_{e-i} = \int_0^\infty \frac{df(E)}{dt} D(E) E dE \equiv \int_0^\infty I_{e-ph} D(E) E dE, \quad (16)$$

where

$$I_{e-ph} = \frac{\pi^3}{\hbar k} \int_0^{E_p} \frac{D_{ph}(E_{ph})}{q} \sum_{\pm} \frac{D(E \pm E_{ph})}{k(E \pm E_{ph})} F^{\pm} M_{e-ph}^2 \Theta_{e-ph} dE_{ph}. \quad (17)$$

$$M_{e-ph}^2 = \frac{e^2}{2\epsilon_0} \frac{E_{ph}}{q^2 + k_{sc}^2}, \quad (18)$$

where M_{e-ph} is the matrix element of the electron–phonon scattering within the jelly-model [20,25], and

$$\Theta_{e-ph} = \begin{cases} 1, & \text{for } [q^2 + k^2 - k^2(E \pm E_{ph})] / (2kq) \in [-1; 1] \\ 0, & \text{otherwise} \end{cases}, \quad (19.1)$$

$$F^{\pm} = f(E \pm E_{ph})[1 - f(E)][g(E_{ph}) + 1/2 \pm 1/2] - f(E)[1 - f(E \pm E_{ph})][g(E_{ph}) + 1/2 \mp 1/2], \quad (19.2)$$

where $g(E_{ph})$ is the phonon Bose-function; E_{ph} and q are the phonon energy and momentum; k is the electron momentum, and $k(E \pm E_{ph})$ is the electron momentum corresponding to the electron energy $E \pm E_{ph}$; $D_{ph}(E_{ph}) = (E_{ph}^2) / (2\pi^2 \hbar^3 v_s^3)$ is the DOS of the longitudinal acoustic phonons within the Debye approximation [19]; $v_s = 6420$ m/s is the sound velocity in aluminum; $E_D = \hbar v_s (6\pi^2 n_{at})^{1/3}$ is the Debye energy; n_{at} is the atomic density. Electron momentum was calculated within an effective one-band dispersion approximation, obtained from DOS of electrons as $k(E) = (3\pi^2 \int_0^E D(\varepsilon) d\varepsilon)^{1/3}$ [19].

5. MD calculation of the DSF

Molecular-dynamic (MD) simulations are applied to obtain the lattice pair correlation function $G(\mathbf{r}, t)$ for aluminum in the classical approximation (4). The original MD code uses the velocity Verlet scheme of the second order [26] with the time-step 1 fs to trace trajectories of atoms. Periodic boundary conditions are applied in the MD algorithm for calculations of forces acting on atoms as well as of the pair correlation function $G(\mathbf{r}, t)$. Standard averaging technique [26] based on the ergodic hypothesis was employed to restore $G(\mathbf{r}, t)$ from the results of MD simulations:

$$G(\mathbf{r}, t) = \frac{1}{N\eta_T} \sum_{\gamma=1}^{\eta_T} \sum_{i,j=1}^N \delta[\mathbf{r} + \mathbf{R}_i(t_\gamma) - \mathbf{R}_j(t_\gamma + t)] , \quad (20)$$

where η_T is the number of time steps of averaging ($\eta_T \approx 10^3$). We varied the distance r from 0 to 30 Å that coincides with the size of the dynamically coupled lattice volume in aluminum (see below), and time t in the range from –10 ps to 10 ps in Eq. (20). The damping function method [27] was used to suppress spurious ripples resulting from truncation of numerical integration in Eq. (3) when calculating the DSF from Eq. (20). Then, the asymmetry modification (5) is introduced for the calculated DSF. This MD algorithm of the DSF calculation was already verified against experimental data in [10].

6. Electron–lattice coupling factor

The charge of aluminum ions in the lattice was considered to be $Z = 3$. Three electrons from each lattice atom gave the concentration $n_e = 1.8 \times 10^{23} \text{ cm}^{-3}$ of the conduction-band electrons in a crystalline aluminum.

Let us mention that the DSF is 4-dimensional function defined for all possible values of \mathbf{k} and ω . Formally, it means that any energy $\hbar\omega$ and momentum $\hbar\mathbf{k}$ can be transferred from a scattering electron to the lattice. But restrictions appear from the applied kinematics and the dispersion laws of particles/quasiparticles participating in scattering events. In the phonon approximation of the lattice dynamics, the maximum energy $\hbar\omega$ and momentum $\hbar\mathbf{k}$ transferred to the lattice in one act of scattering are limited by the maximum phonon wave vector \mathbf{k}_{ph}^{\max} and maximum phonon energy $\hbar\omega_{ph}^{\max}$. To account in the integration of Eq. (6) (the electron–lattice energy exchange rate Q_{e-i}), we split the electron energies into two intervals. For electrons with energies lower than a threshold energy E_{thr} ($E_k < E_{thr}$), which means the interaction times with the dynamically coupled volume are larger than the atomic vibration time, the maximum wave vector \mathbf{k} and energy $\hbar\omega$ transferred to the lattice are restricted by the maximum wave vector and the energy of a phonon in the lattice. In the “instantaneous” approximation of the lattice dynamics for scattering of electrons with the larger electron energies ($E_k > E_{thr}$), we do not assume limitations additional to those of the kinematics of a binary collision.

To estimate the size of the dynamically correlated volume for aluminum, we calculated mean scalar product of displacements

of atoms from their equilibrium positions depending on the distance between these atoms. The product is not equal to zero (correlated atomic dynamics) when this distance does not exceed $l_{corr} \approx 30$ Å (7-cells). The maximum (threshold) value of the interaction time necessary for realization of the instantaneous approximation was chosen much shorter than the atomic vibration time $t_{inst} \approx 1 \text{ fs} \ll (\omega_{osc})^{-1}$. For this time t_{inst} and the correlation length $l_{corr} \approx 30$ Å, the threshold electron energy $E_{thr} \approx 15$ eV separates the phonon and instantaneous approximations of the dynamic response of the lattice of aluminum. Taking this into account, we apply the “phonon restrictions” in the integration limits in Eq. (6) with MD-calculated DSF of aluminum when $E_k < 15$ eV and the “binary-encounter” limits for $E_k > 15$ eV.

The electron–lattice coupling factor is commonly used in TTM to characterize the electron–ion energy transfer rate [17]:

$$g_{e-i} = -\frac{\partial E}{\partial t} \cdot \frac{1}{T_e - T_i} = Q_{e-i} \cdot \frac{1}{T_e - T_i} . \quad (21)$$

Fig. 3 presents comparison of the MD calculated electron–lattice coupling factor with those calculated under harmonic and instantaneous approximations. This figure demonstrates that the behavior of the coupling factor based on MD-DSF is very similar to its harmonic approximation at $T_e < 10^4$ K. At $T_e > 3 \cdot 10^5$ K, the g -factor based on MD-DSF is similar to that calculated in the framework of the instantaneous approximation (plasma limit). The temperature dependence of the electron–lattice coupling factor based on MD-DSF in the transitional region $10^4 \text{ K} < T_e < 3 \cdot 10^5 \text{ K}$ differs from the both limit cases.

Fig. 4 compares the electron–lattice coupling factors calculated in the phonon-approximation of [17,19] for Al at the lattice temperature $T_i = 300$ K with the results of MD-DSF calculations. The experimental data [28–30] are also shown in Fig. 4.

One can also see in Fig. 4 that the results of application of the electron–phonon approximation, curve (3), are similar to the MD-DSF calculations, curve (1), only in the intermediate region ($10^3 \text{ K} - 10^4 \text{ K}$). Indeed, for the higher electron temperatures, the DSF-obtained transition to the plasma limit is not recovered within the phononic approximation. On the other hand, on lower temperatures, the MD-DSF calculations take into account all the anharmonicities, as mentioned above. As a result, the phononic approximation decreases much faster with decrease of the electron temperature.

The results demonstrate that our MD-DSF curve (1) exceeds the experimental points and curves calculated by other groups by a factor of two or three at low electron temperatures ($T_e < 10^4 \text{ K}$). This difference can be related to the following:

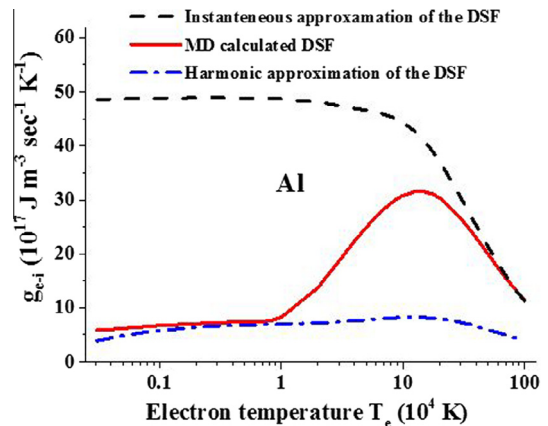


Fig. 3. Electron–lattice coupling factor in aluminum as a function of the electron temperature obtained within different approximations.

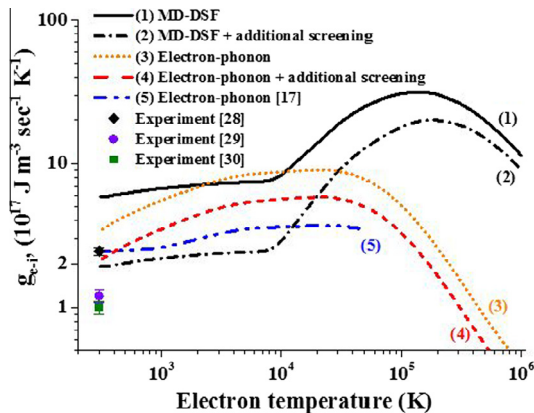


Fig. 4. The electron–lattice coupling factor in aluminum measured in experiments vs those calculated in the framework of different models.

- The experimental points from [29,30] (g_{e-l} – factor at $T_e = T_i = 300$ K) differ by more than a factor of two from that obtained in the experiment [28] and from all the calculations. It can be, perhaps, associated with different techniques used in [28–30] and with various parameters of the laser sources applied in these experiments in order to extract g_{e-l} – factor. It should also be noted that the model assumptions (based on the two-temperature model) were used in order to extract the value of the g_{e-l} – factor from the experimental raw data in [28–30]. Therefore, independent verifications and/or analyses of the experimental results are very desirable.
- The authors of [17] used the experimental point from [28] to adjust their calculated g_{e-l} – factor at $T_e = T_i = 300$ K, shown in Fig. 4 as curve (5).
- MD-DSF procedure takes into account all the possible collective modes of the lattice: phonons, anharmonic contributions to the lattice dynamics, etc., that increase, in comparison to [17] and [19], electron–lattice coupling at low electron temperatures ($T_e < 10^4$ K).
- It was demonstrated in [22] that effects of coupled modes (an interaction of collective electronic modes with collective atomic modes) provide an additional screening of electron–atom interaction. Our calculations match the experimental points when taking into account this effect by multiplying the square of the inverse electronic screening length (Eq. (9)) by a factor of 2, as it was done in [19]; compare the curve (2) to the original curve (1) in Fig. 4. The same is done also for calculation in our phononic approximation for comparison, which also significantly improves its coincidence with experimental points, see curve (4) vs curve (3).

At last, we should mention that the present model assumes constant electron density in the conduction band of aluminum. For the electron temperatures above $\sim 5 \times 10^5$ K ionization of L-shell of aluminum starts (ionization potential is 72.6 eV [31]). Therefore, although our model demonstrates correct transition to the instantaneous approximation (plasma) limit, in practical applications of the model possible variations in the electron density at high electron temperatures must be included (by means of, e.g. Saha equation).

7. Conclusions

The parameters of highly excited ensemble of electrons in the conduction band of aluminum (the electron heat capacity, the

screening length and the chemical potential) are calculated from the realistic density of states. Dependence of the electron–lattice coupling factor on the temperature of the electron ensemble is demonstrated. The different branches of this dependence occur due to different dynamical responses of a lattice to excitations by scattering electrons of different energies. The dynamic structure factor (DSF) formalism is applied to describe this effect. The DSF formalism takes automatically into account different collective response of the lattice in electron–lattice coupling.

It is shown that the simplest electron–phonon approximation fails dramatically on high electron temperatures tending to the “plasma-limit”, while also being incomplete for low electron temperatures.

Comparison with available experimental data demonstrates that the effect of additional screening of the electron–lattice potential due to interaction of electron and lattice coupled modes plays an important role, reducing the electron–ion energy exchange rate.

The presented calculated parameters can be used in two-temperature modeling. The DSF-based procedure can be introduced as an independent module into models and codes describing lattice excitation and structure transformations in materials irradiated with swift-heavy ions or intense laser pulses.

Acknowledgement

Financial support from grant 13-02-1020 ofi-m from Russian Foundation for Basic Research (Russia) is acknowledged by S.A. Gorbunov and A.E. Volkov.

References

- A.M. Miterev, Phys. Usp. 172 (2002) 1131.
- L.T. Chadderton, Radiat. Meas. 36 (2003) 13.
- B. Nagler, U. Zastra, R.R. Fäustlin, S.M. Vinko, T. Whitcher, A.J. Nelson, R. Sobierajski, J. Krzywinski, J. Chalupsky, E. Abreu, S. Bajt, T. Bornath, T. Burian, H. Chapman, J. Cihelka, T. Döppner, S. Düsterer, T. Dzelzainis, M. Fajardo, E. Förster, C. Fortmann, E. Galtier, S.H. Glenzer, S. Göde, G. Gregori, V. Hajkova, P. Heimann, L. Juha, M. Jurek, F.Y. Khattak, A.R. Khorsand, D. Klinger, M. Kozlova, T. Laarmann, H.J. Lee, R.W. Lee, K.-H. Meiwes-Broer, P. Mercere, W.J. Murphy, A. Przystawik, R. Redmer, H. Reinholz, D. Riley, G. Röpke, F. Rosmej, K. Saksl, R. Schott, R. Thiele, J. Tiggesbäumker, S. Toleikis, T. Tschentscher, I. Uschmann, H.J. Vollmer, J.S. Wark, Nat. Phys. 5 (2009) 693.
- U. Zastra, C. Fortmann, R. Fäustlin, L. Cao, T. Döppner, S. Düsterer, S. Glenzer, G. Gregori, T. Laarmann, H. Lee, A. Przystawik, P. Radcliffe, H. Reinholz, G. Röpke, R. Thiele, J. Tiggesbäumker, N. Truong, S. Toleikis, I. Uschmann, A. Wierling, T. Tschentscher, E. Förster, R. Redmer, Phys. Rev. E 78 (2008) 066406.
- S.M. Vinko, U. Zastra, S. Mazevet, J. Andreasson, S. Bajt, T. Burian, J. Chalupsky, H.N. Chapman, J. Cihelka, D. Doria, T. Döppner, S. Düsterer, T. Dzelzainis, R.R. Fäustlin, C. Fortmann, E. Förster, E. Galtier, S.H. Glenzer, S. Göde, G. Gregori, J. Hajdu, V. Hajkova, P.A. Heimann, R. Irsig, L. Juha, M. Jurek, J. Krzywinski, T. Laarmann, H.J. Lee, R.W. Lee, B. Li, K.-H. Meiwes-Broer, J.P. Mithen, B. Nagler, A.J. Nelson, A. Przystawik, R. Redmer, D. Riley, F. Rosmej, R. Sobierajski, F. Tavella, R. Thiele, J. Tiggesbäumker, S. Toleikis, T. Tschentscher, L. Vysin, T.J. Whitcher, S. White, J.S. Wark, Phys. Rev. Lett. 104 (2010) 225001.
- N. Medvedev, U. Zastra, E. Förster, D.O. Gericke, B. Rethfeld, Phys. Rev. Lett. 107 (2011) 165003.
- M.I. Kaganov, I.M. Lifshitz, L.V. Tanatarov, Sov. Phys. JETP 4 (1957) 173.
- V.L. Ginzburg, V.R. Shabanskiy, Dokl. Akad. Nauk SSSR 100 (1955) 445 (in Russian).
- A.E. Volkov, V.A. Borodin, Nucl. Instr. Meth. Phys. Res. Sect. B 146 (1998) 137.
- S.A. Gorbunov, N.A. Medvedev, P.N. Terekhin, A.E. Volkov, Nucl. Instr. Meth. Phys. Res. Sect. B 315 (2013) 173.
- L. Van Hove, Phys. Rev. 95 (1954) 249.
- R. Aamodt, K.M. Case, M. Rosenbaum, P.F. Zweifel, Phys. Rev. 126 (1962) 1165.
- T. Scopigno, U. Balucani, G. Ruocco, F. Sette, Phys. Rev. E 63 (2000) 011210.
- D.J. González, L.E. González, J.M. López, M.J. Stott, J. Chem. Phys. 115 (2001) 2373.
- R. Gerald, A. Geiger, Mol. Phys. 70 (1990) 465.
- J.P. Hansen, I.R. McDonald, Theory of Simple Liquids, Academic Press, London, 2006. p. 204.
- Z. Lin, L.V. Zhigilei, V. Celli, Phys. Rev. B 77 (2008) 075133.
- Y. Rosenfeld, G. Chabrier, J. Stat. Phys. 89 (1997) 283.
- B.Y. Mueller, B. Rethfeld, Phys. Rev. B 87 (2013) 035139.
- N.W. Ashcroft, N.D. Mermin, Solid state physics, in: Harcourt (Ed.), Saunders College Publishing, USA, 1976. p. 204.
- B.Y. Mueller, I. Klett, B. Rethfeld, AIP Conf. Proc. 1464 (2012) 609.

- [22] M.W.C. Dharma-Wardana, F. Perrot, Phys. Rev. E 58 (1998) 3705.
- [23] W. Montfrooij, P. Verkerk, I. de Schepper, Phys. Rev. A 33 (1986) 540.
- [24] S. Jenö, Fundamentals of the Physics of Solids, vol. 1, Springer-Verlag, Berlin, Heidelberg, 2007, p. 442.
- [25] D. Pines, Elementary Excitations in Solids, Perseus Books Publishing, L.L.C., Massachusetts, 1999, p. 239.
- [26] M. Rieth, Nano-Engineering in Science and Technology, World Scientific Publishing Co., Pte. Ltd., USA, 2003, p. 54.
- [27] Z. Lin, L.V. Zhigilei, Phys. Rev. B 73 (2006) 184113.
- [28] J.L. Hostetler, A.N. Smith, D.M. Czajkowsky, P.M. Norris, Appl. Opt. 38 (1999) 3614.
- [29] Z. Li-Dan, S. Fang-Yuan, Z. Jie, T. Da-Wei, Acta Phys. Sin. 61 (2012) 134402.
- [30] W. Ma, H. Wang, X. Zhang, W. Wang, International Journal of Thermophysics, in: Special Conference Issue: Selected Papers of the Ninth Asian Thermophysical Properties Conference, 34 (2013) 2400.
- [31] M. Cardona, L. Ley, Photoemission in Solids I: General Principles, Springer-Verlag, Berlin, 1978, p. 149.